Leptons with energy >200 MeV trapped near the South Atlantic Anomaly

E. Fiandrini, G. Esposito, B. Bertucci, B. Alpat, G. Ambrosi, R. Battiston, W. J. Burger, D. Caraffini, C. Cecchi, L. Di Masso, N. Dinu, M. Ionica, R. Ionica, G. Lamanna, M. Pauluzzi, M. Menichelli, and P. Zuccon

Department of Physics, Perugia University, Perugia, Italy

Istituto Nazionale di Fisica Nucleare, Rome, Italy

Received 15 January 2003; revised 4 June 2003; accepted 4 August 2003; published 20 November 2003.

[1] Accurate measurements of electron and positron fluxes in the energy range 0.2–10 GeV have been performed with the Alpha Magnetic Spectrometer (AMS) at altitudes of 320–390 km in the geographic latitude interval ±51.7°. We focus on the fluxes measured in the regions nearby the South Atlantic Anomaly, defined by the local magnetic values of the magnetic field B ($0.21 \leq B \leq 0.26$ G) at the altitude of AMS. A clear transition from the Stably Trapped population typical of the Inner Van Allen belts to Quasi-Trapped population in the regions underneath the Van Allen belts is observed. The high energy observations demonstrate the relatively higher abundance of positrons in the Inner Van Allen belts, for both the Stably Trapped and the Quasi-Trapped populations. The flux maps as a function of the canonical adiabatic variables L, α_o are presented for the interval $0.95 < L < 3$, $0° < \alpha_o < 90°$ for electron energies below 10 GeV and positrons energies below 3 GeV. The results are compared with existing data at lower energies. *INDEX TERMS:* 2720 Magnetospheric Physics: Energetic particles, trapped; 2716 Magnetospheric Physics: Energetic particles, precipitating; 2736 Magnetospheric Physics: Magnetosphere/ionosphere interactions; 2730 Magnetospheric Physics: Magnetosphere—inner; 2116 Interplanetary Physics: Energetic particles, planetary; *KEYWORDS:* leptons, South Atlantic Anomaly

Citation: Fiandrini, E., et. al., Leptons with energy >200 MeV trapped near the South Atlantic Anomaly, *J. Geophys. Res.*, *108*(A11), 1402, doi:10.1029/2003JA009844, 2003.

1. Introduction

[2] The presence of trapped electrons and positrons (up to few hundred MeV) in the Inner Van Allen (IVA) belts is well established. The existing experimental data in the energy range of 0.04–200 MeV come from satellites covering a large range of adiabatic variables [*Voronov et al.*, 1986, 1987; *Galper et al.*, 1986; *Akimov et al.*, 1987; *Heynderickx et al.*, 1996].

[3] Although the principal processes responsible for the belts are known, a complete model of the sources and losses, the energy spectra, and the spatial distribution of the particle populations does not exist [*Gusev and Pugacheva*, 1982; *Voronov et al.*, 1995; *Derome et al.*, 2000; *Huang*, 2003] (P. Zuccon, A Monte Carlo Simulation of the cosmic rays interactions with the near Earth environment, unpublished, http://ams.pg.infn.it/Tesi/Tesi.html, 2002). This is particularly true for the region of the South Atlantic Anomaly (SAA) where the inner belts approach the atmosphere. The study of the high-energy component of the trapped flux in this region is important for radiation belt models, for the determination of the radiation dose for satellites and manned spacecraft [*Badhwar et al.*, 2001], and for the determination of backgrounds for space and ground experiments.

[4] At low energies, there exist models of the radiation belts for electrons up to a few MeV and for protons up to hundreds of MeV, based on the data provided by the long duration satellite campaigns of the NASA Trapped Radiation Environment Program (TREP), AE-8 and AP-8 [*Vette*, 1991]. The models are continually updated in the context of the Trapped Radiation Environment Development (TREND) project (http://www.magnet.oma.be/home/trend-trend.html, http://www.magnet.oma.be/unilib.html, http://www.spenvis.oma.be/spenvis) and the Space Weather Program of NASA.

[5] At higher energies (above a few MeV and below a few tens of MeV), trapped lepton data were provided by the spaceborne missions of the Moscow Engineering Physics Institute (MEPHI) during the 1970s and 1980s. The data were accumulated by different satellites (Proton, Cosmos, Salyut, Gamma series) and MIR [*Averin et al.*, 1988; *Galper et al.*, 1996; *Galper et al.*, 1986; *Akimov et al.*, 1987; *Voronov et al.*, 1987]. The satellites, with orbital altitudes ranging between 300 and 1000 km, collected data both inside and outside the SAA. The ratio of e^+ to e^- is found to be very strongly dependent on the location in the magnetic field. In the SAA the measured e^- are found to be a factor of 10 larger than e^+, while outside the ratio of the two lepton

0148-0227/03/2003JA009844

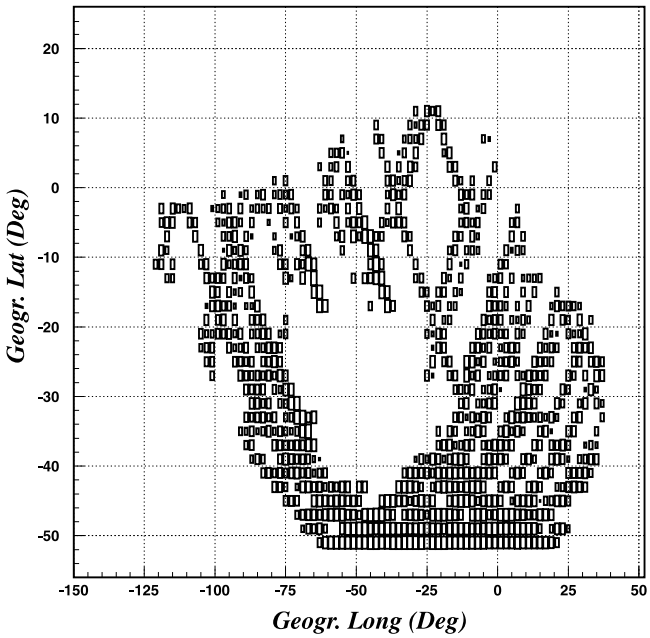

Figure 1. Alpha Magnetic Spectrometer (AMS) measurements in the region where the local magnetic field B is less than 0.26 G at the altitude of the AMS during STS-91 flight. The South Atlantic Anomaly (SAA) region is defined by this region. The empty region in the core of SAA, corresponding to field values $B \leq 0.21$ G, is due to the zero lifetime of the detector.

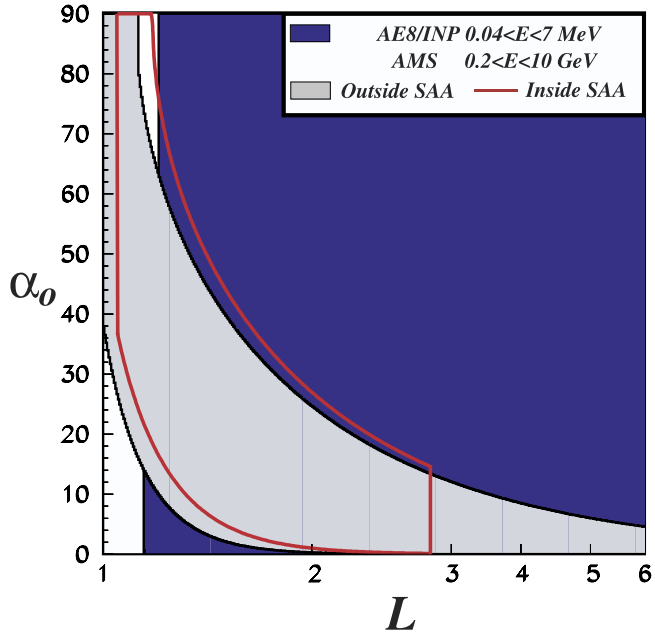

Figure 2. Comparison of the field of view of AMS inside (contour) and outside (open region) SAA with the current NASA/Institute of Nuclear Physics coverage (blue region) in (L, α_o) phase space.

fluxes is close to 1 (V. V. Mikhailov, private communication, 2001), [*Galper et al.*, 1996].

[6] At energies above few hundreds of MeV, below the geomagnetic cutoff, accurate measurements of leptons have been performed by AMS in low Earth orbit. The AMS data collected outside the SAA have been analyzed and compared with lower-energy measurements taken at similar altitudes [*Fiandrini et al.*, 2002]. In this paper, we use the high statistics data sample collected by the AMS experiment for a detailed study of the high-energy (O(1 GeV)) lepton fluxes nearby the SAA region, excluded in the previous publication.

[7] In general, the SAA region is not sharply defined [*Fung*, 1996; *Lemaire et al.*, 1998]. Here it is defined as the region where the local magnetic field B is $\leq$0.26 G, corresponding to the geographic region shown in Figure 1. This definition is of general use and does not correspond to a physical separation of the drift shells [e.g., *Galper et al.*, 1996]. The data are analyzed in terms of the canonical invariant coordinates characterizing the particle motion in the magnetic field: the L shell parameter, the equivalent magnetic equatorial radius of the shell, and the equatorial pitch angle (α_0) between the momentum $\vec{p}$ and field $\vec{B}$ [*McIlwain*, 1961; *Hilton*, 1971].

2. AMS Data Analysis

[8] The Alpha Magnetic Spectrometer (AMS) was operated on the shuttle Discovery during a 10-day flight, beginning on 2 June 1998 (NASA mission STS-91). The orbital inclination was 51.7° in geographic coordinates, at a geodesic altitude of 320–390 km. The detector, not magnetically stabilized, recorded data at different fixed attitudes with respect to the local zenith direction (0°, 20°, 45°, and 180°). The data relevant to the present analysis represent 8.2 hours in the regions nearby the SAA and 37.5 hours in the region outside of SAA. Details on the detector performance, lepton selection, and background estimation can be found in the work of *Alcaraz et al.* [2000].

[9] The values of L, α_0 of the detected leptons were calculated using the UNILIB package (TREND, http://www.magnet.oma.be/home/trend-trend.tml, http://www.magnet.oma.be/unilib.html, http://www.spenvis.oma.be/spenvis) with a realistic magnetic field model, including both the internal and the external contributions (IGRF, available at http://nssdc.gsfc.nasa.gov/space/model/models/igrf.html) [*Tsyganenko*, 1982]; details can be found in the work of *Fiandrini et al.* [2002] and G. Esposito (Study of cosmic ray fluxes in low earth orbit observed with the AMS experiment, http://ams.pg.infn.it/Tesi/Tesi.html, 2002). The AMS Field of View (FoV) along the orbits in the SAA is shown in Figure 2. It should be pointed out that although the geographical area corresponding to the region of the SAA is rather limited (Figure 1), the L, α_0 coverage is about the same as outside due to the fact that at the edge of the SAA the drift shells drop to very low altitudes.

Table 1. Statistics of the Alpha Magnetic Spectrometer Data Used in This Work

	e^+	e^-	Time(s)
ST $B \leq 0.26$ G	2960	1785	29,540
QT $B \leq 0.26$ G	10,683	4990	
ST $B \geq 0.26$ G	0	0	135,000
QT $B \geq 0.26$ G	46,517	18,487	

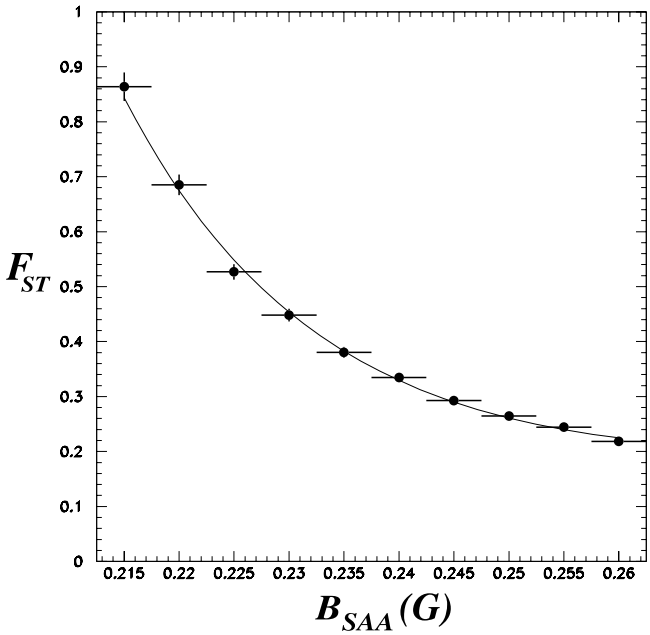

Figure 3. Fraction of Stably Trapped population with respect to the total as a function of the maximum local magnetic field B_{SAA}, used to define SAA contours. The power law used for the fit is superimposed.

[10] Useful trigger rates varied between 100 and 700 Hz, attaining a maximum rate in the core of the SAA where detector lifetime went to zero. Data analyzed in this paper correspond to a detector trigger efficiency $\geq$90% and lifetime $\geq$30%. The zero-lifetime region appears in Figure 1 in the center of the SAA and corresponds to magnetic field intensities $B < 0.21$ G. Therefore, the more central region of the SAA is not observed, and the term "inside the SAA" is used in the following to denote the regions where $0.21 < B < 0.26$ G.

2.1. Particle Classification

[11] To reject the primary component of the measured lepton fluxes, the lepton trajectories in the Earth's magnetic field were traced in a realistic geomagnetic field model with the Earth's penumbra effects taken into account [*Fiandrini et al.*, 2002] (G. Esposito, http://ams.pg.infn.it/Tesi/Tesi.html, 2002). Particles are classified as cosmic if they reach a distance of 30 Earth radii. The remaining particles, classified as secondaries, may reach the Earth's atmosphere at some point of the trajectory (Quasi-Trapped (QT)) or remain in flight around the Earth for at least a complete drift (Stably Trapped (ST)), corresponding to a maximum time period of 30 s at the energies relevant for our data. In our case, if a particle travelled for 30 s, it will likely travel indefinitely. The notation "Quasi-Trapped" was used by

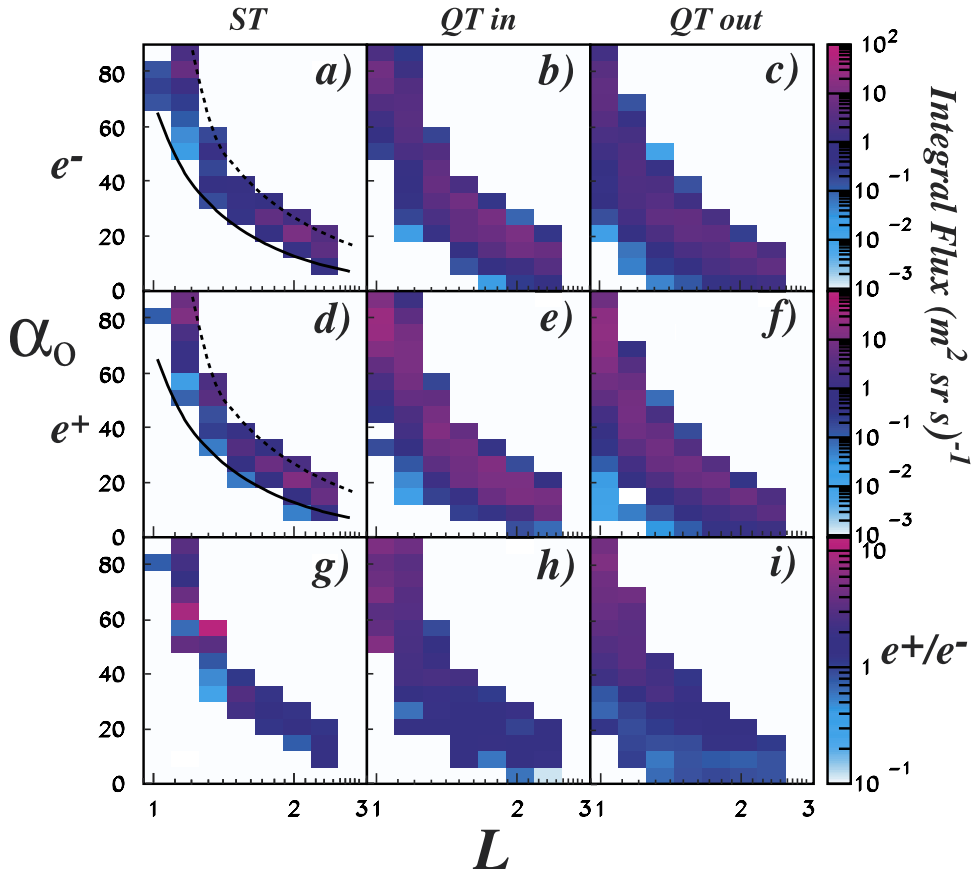

Figure 4. Integral flux in the interval 0.205–2.73 GeV for (a) Stably Trapped, (b) Quasi-Trapped in SAA and (c) Quasi-Trapped outside the SAA electrons; for (d) Stably Trapped, (e) Quasi-Trapped in SAA, and (f) Quasi-Trapped outside the SAA positrons. The corresponding charge ratios are shown in Figures 4g, 4h, and 4i, respectively. The curves show the limit for the full Inner Van Allen belts, the full lines show the limit for stable trapping at AMS orbit altitude, as explained in text.

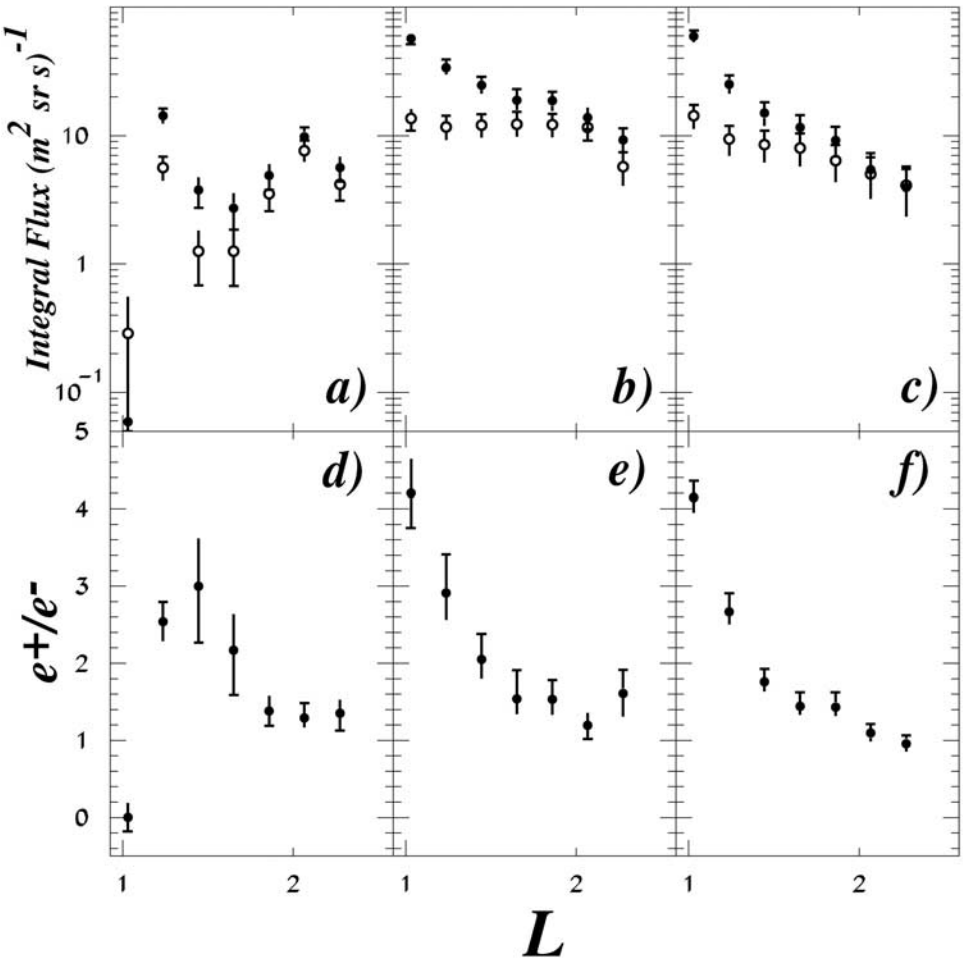

Figure 5. Flux integrated over α_0 in the interval 0.205–2.73 GeV as a function of L shell parameter for Stably Trapped and Quasi-Trapped components in SAA and Quasi-Trapped flux outside SAA is shown in Figures 5a, 5b, and 5c, respectively. Open and solid circles show electrons and positrons, respectively; the corresponding charge ratios are shown in Figures 5d, 5f, and 5e, respectively. The errors take into account both the statistical and the systematic errors induced by the experimental uncertainties. The sign and size of the systematic errors are given by the small pin in the errors' bar end.

Fiandrini et al. [2002] to denote particles with residence times in the belts $0.3 < T_f < 30$ s; here it is used to denote all the particles with $T_f < 30$ s.

[12] For a proper selection of trapped particles as generally intended in radiation belts physics, it is required to have particles which are classified as secondaries by the tracing and which satisfy the kinematical conditions for the adiabatic description, according to the smallness parameter ϵ [*Il'in et al.*, 1986]. To remove possible nonadiabatic, nonlinear behaviors in the particle populations, two effective cutoffs were defined: an upper cutoff R_{cu}, defined as the highest rigidity above which all the particles are cosmic, and a lower cutoff R_{cl} as the lowest rigidity below which all the particles are secondaries. The region between R_{cl} and R_{cu} defines the penumbra region where the adiabatic approach does not hold and the particle trajectories are highly chaotic with nonlinear dependence on the initial conditions so that the particle classification is uncertain. For this reason, all the particles with $R > R_{cl}$ were rejected even if classified as secondaries from tracing. To check the goodness of the effective cutoff, upgoing (attitude180°) and downgoing (attitude 0°) fluxes were computed separately. The upgoing flux was unchanged after the rigidity cutoff application, as expected, because no cosmic and penumbral flux is present. In the downgoing flux, all the components are present, but after the effective cutoff, only secondary flux outside the penumbra is left. This agrees very well with the upgoing one, since secondary upgoing and downgoing fluxes are the same population of particles (i.e., with equivalent pitch angles on the same field lines), as expected from a correct removal of penumbral and cosmic particles. The adiabaticity conditions were cross-checked with the smallness parameter ϵ, which has to be below a critical limit (<0.1); all the particles below the effective cutoff R_{cl} fulfill the condition and have regular motion, while all the particles in the penumbra region and the cosmic component have large values. In this sense the effective cutoff R_{cl} is equivalent to the critical limit of the smallness parameter ϵ.

[13] Table 1 reports the number of QT and ST secondaries collected by AMS inside the region where $B < 0.26$ G and outside of it. A relevant feature is that the ST component is

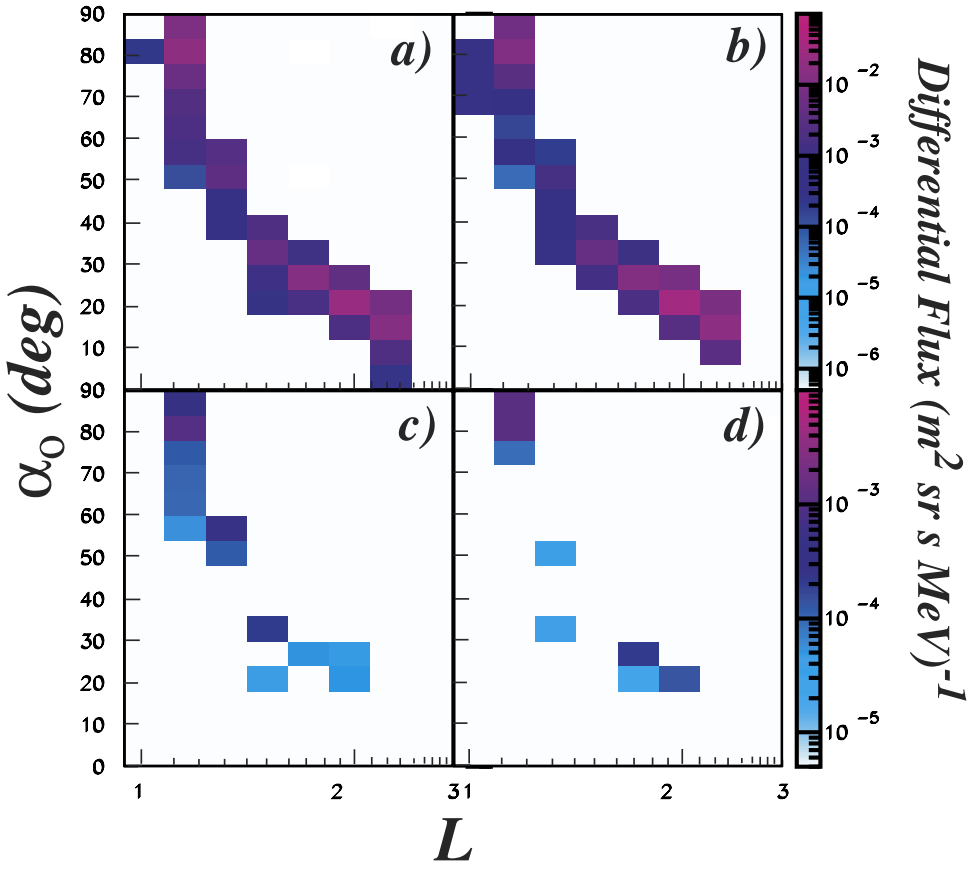

Figure 6. (a, c) The e^+ and (b, d) e^- differential flux maps for the Stably Trapped (ST) component inside the SAA, for the energy bins $0.2 \leq E \leq 0.315$ GeV (Figures 6a and 6b) and $0.75 \leq E \leq 1.15$ GeV (Figures 6c and 6d).

found only when B < 0.26 G, while QT are detected everywhere. We reported previously the results for the QT component outside the SAA in the work of *Fiandrini et al.* [2002] in which the region B < 0.26 G was completely excluded and no ST particles were observed.

2.2. Transition From Stably Trapped to Quasi-Trapped

[14] It is interesting to study the transition profile of the QT and ST populations as a function of the geomagnetic field value, B_{SAA}, used to define the SAA contour. The fraction of the ST component was defined as $F_{ST}(B_{SAA}) = J_{st}(B_{SAA})/J_{tot}(B_{SAA})$, where $J(B_{SAA}) = \int_{B \leq B_{SAA}} j_{int} dB$ is the integral flux measured in the region where $B \leq B_{SAA}$, and j_{int} is the total flux of a given component and it is shown in Figure 3. Below $B_{SAA} = 0.26G$ the fraction of Stably Trapped component F_{st} can be described with the law $F_{st} = 1 - (B_{SAA}/B_o)^{-\alpha} + (B_{SAA}/B_o)^{-\beta}$, with $B_0 = 0.211 \pm 0.008$ G, $\alpha = 0.593 \pm 0.085$ and $\beta = 10.696 \pm 0.658$; the Quasi-Trapped fraction is $F_{qt} = 1 - F_{st}$. B_o is the field value at which the flux becomes entirely Stably Trapped ($F_{st} = 1$) and represents the limit of the full IVA belts at the altitude of the AMS orbit. Above 0.26 G, F_{st} becomes constant, indicating that j_{st} vanishes and the flux is only QT.

[15] The AMS deadtime in the SAA limits the observable field to B > 0.21 G. Therefore we cannot observe the full closed IVA belts but rather the transition region between the IVA belts and the underlying region, where the drift shells are not closed, which we refer to as "mixed radiation belt" (MRB).

[16] Because of the observed mixing between QT and ST components, the MRB region could be, at least partly, responsible for the filling and depletion of the IVA belts, due to pitch angle scattering by elastic interactions with the residual atmosphere.

3. AMS Results

[17] The total energy E, the L shell parameter and the equatorial pitch angle α_0 are used to describe the fluxes. The pitch angle is preferred to B_m since it is limited to 0°/90°. A three-dimensional grid (E, L, α_0) is defined to build flux maps as in the work of *Fiandrini et al.* [2002].

[18] Flux maps as a function of (L, α_o) integrated over the energy interval $0.2 \leq E \leq 2.73$ are shown in Figure 4. The QT and ST components measured inside the SAA and the QT component measured outside the SAA are shown separately for e^- and e^+ in Figures 4a, 4b, and 4c and 4d, 4e, and 4f, respectively. The corresponding positron to electron ratios are plotted in Figures 4g, 4h, and 4i.

[19] The QT fluxes inside and outside SAA look similar. They both cover the full (L, α_0) phase space accessible to AMS with similar intensities (Figures 4b, 4c, 4e, and 4f) and also the charge composition is basically the same in the two populations as seen in Figures 4h and 4i, where a

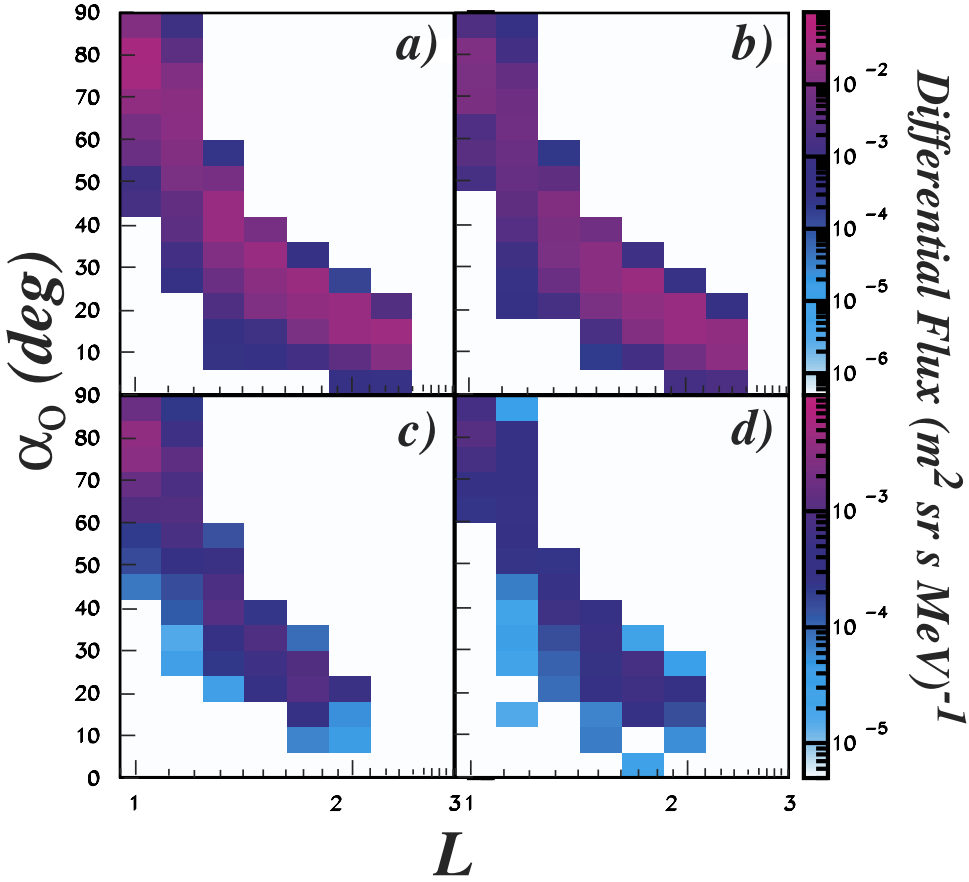

Figure 7. (a, c) The e^+ and (b, d) e^- differential flux maps for the Quasi-Trapped (QT) component inside the SAA, for the energy bins $0.2 \leq E \leq 0.315$ GeV (Figures 7a and 7b) and $0.75 \leq E \leq 1.15$ GeV (Figures 7c and 7d).

maximum at same L and α_o is observed. This is an indication that the same particle population is observed in different locations of the same drift shells inside and outside the SAA.

[20] A different behavior characterizes the ST component, which is contained in the narrow band delimited by the solid and dashed lines in Figures 4a and 4d. The solid lines represent the lower limit for the Stably Trapped component at the altitude of AMS, described with the relation $sin\alpha_{st} = AL^{-\beta}$, with $A = 0.97 \pm 0.05$ and $\beta = 1.76 \pm 0.12$. This is the limit for stable trapping in the IVA belts, in the sense that particles with $\alpha_o < \alpha_{st}$ cannot be injected into the IVA belts; the angle α_{st} can be defined as the "equatorial drift loss cone angle". The dashed lines correspond to the upper limit for the IVA belts at the altitude of AMS, given by $\sin\alpha_{IVA} = \sqrt{0.311/B_oL^3}$, with $B_o = 0.21$ G, the value found in the fit for ST fraction F_{ST} (Figure 3). The region between the two curves represents the MRB region at the altitude of AMS. The charge composition map of ST flux shows a peculiar structure, with a positron dominance and a clear peak at $L \sim 1.2$ and $\alpha_o \sim 60°$ (Figure 4g).

[21] The similarity of the QT fluxes observed inside and outside the SAA and the different behavior of the ST flux are evident also in the radial distributions presented in Figure 5. The upper plots show the L dependence of e^+ and e^- fluxes after integration over α_0 for the ST (Figure 5a) and QT components inside (Figure 5b) and outside (Figure 5c) the SAA. The positron to electron charge ratio as a function of L is shown for each population in the lower plots (Figures 5d, 5e, and 5f).

[22] The distributions of QT fluxes (Figures 5b and 5c) as well as their charge ratio (Figures 5e and 5f) are similar inside and outside the SAA. On the other hand, the ST fluxes show a clear dependence on L for both electrons and positrons (Figure 5a), with two maxima at $L \sim 1.2$ and ~ 2.1 and a minimum at $L \sim 1.4$. A maximum in the positron to electron ratio (Figure 5d) is observed in correspondence of the ST flux minimum. Further differences among QT and ST components of the flux are found in the analysis of their spectral behavior.

[23] Two differential flux maps at constant E as a function of (L, α_0) are given in Figures 6 and 7, for the ST and QT leptonic components inside the SAA and in Figure 8 for the QT flux outside the SAA. In Figures 6 to 8, panels a and c refer to e^+ flux for $0.205 \leq E \leq 0.315$ GeV and $0.75 \leq E \leq 1.15$ GeV, respectively; panels b and d refer to the same energy intervals for e^-.

[24] For both e^+ and e^-, the ST component is concentrated at low energies, as it can be seen from the different intensities and phase space coverage in the low (Figures 6a and 6b) and high (Figures 6c and 6d) energy maps of Figure 6. Trapping becomes very unlikely for particles with E above several hundreds of MeV. This is consistent with a relative suppres-

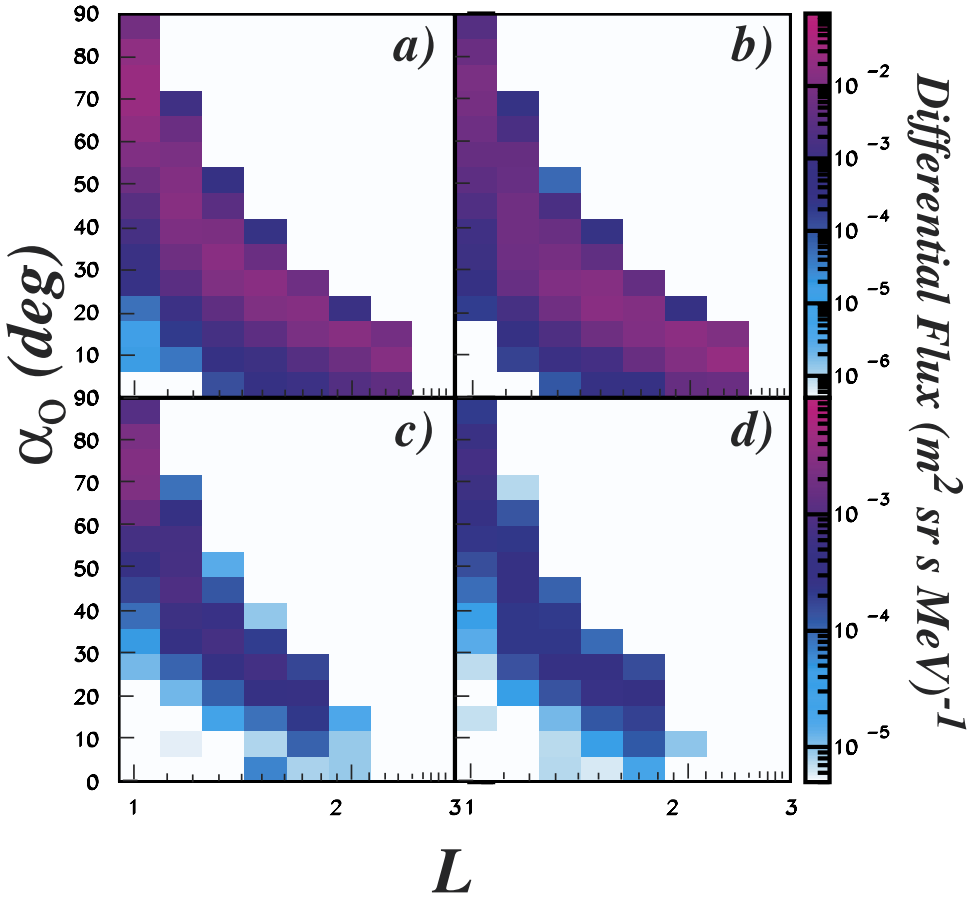

Figure 8. (a, c) The e^+ and (b, d) e^- differential flux maps for the QT component outside the SAA, for the energy bins $0.2 \leq E \leq 0.315$ GeV (Figures 8a and 8b) and $0.75 \leq E \leq 1.15$ GeV (Figures 8c and 8d).

sion at high energies of injection mechanisms based on pitch angle diffusion due to Coulomb scattering.

[25] The energy dependence of the different flux components can be better seen in Figure 9. The differential flux at low L ($\leq$1.2) and high equatorial pitch angles ($\alpha \geq 70°$) is separately shown for e^+ (Figures 9a and 9c) and e^- (Figures 9b and 9d). Upper plots (Figures 9a and 9b) refer to the QT flux outside the SAA while the QT and ST components inside the SAA are shown in the lower panels (Figures 9c and 9d). The charge ratio of the same data is shown as a function of energy in Figure 10 outside (Figure 10a) and inside (Figure 10b) the SAA. There is a clear positron dominance in all the components observed by AMS, ST, and QT inside the SAA and also in the QT component outside the SAA. The energy dependence of the two fluxes (ST and QT) is different: The ST component is softer than the QT one for both electrons and positrons, a strong indication of an energy limitation for the stable trapping in Van Allen belts. The differential QT fluxes inside and outside the SAA have similar composition, slopes and comparable intensities, giving a further support to their common origin. This allows to drop the distinction

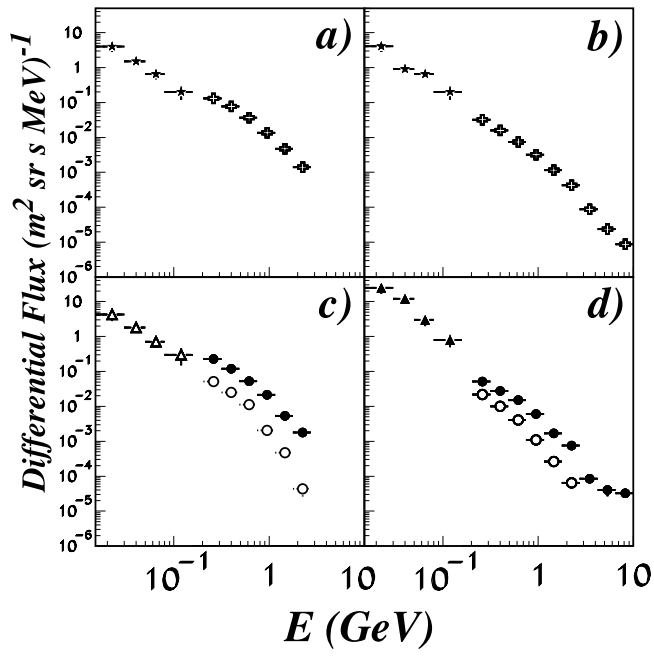

Figure 9. (opposite) (a, c) Differential flux of positrons and (b, d) electrons in the region $L \leq 1.2$ and $\alpha_o \geq 70°$. Triangles and stars show Marya data inside and outside the SAA, respectively. Solid and open circles show AMS Quasi-Trapped and Stably Trapped component inside the SAA, respectively. The crosses show the Quasi-Trapped component outside the SAA, measured by AMS.

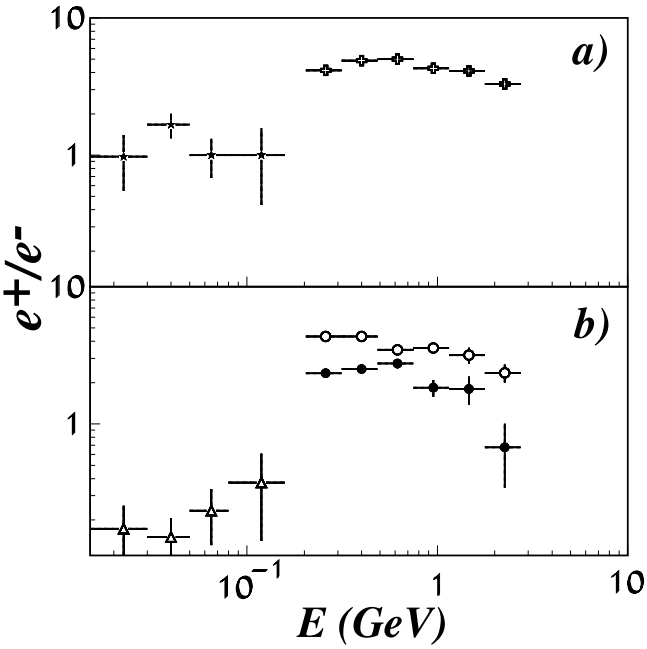

Figure 10. Charge ratio of positrons to electrons (a) outside and (b) inside the SAA in the region $L \leq 1.2$ and $\alpha_o \geq 70°$. Triangles and stars show the ratio for Marya data inside and outside the SAA, respectively; the open and solid circles show the measured AMS Quasi-Trapped and Stably Trapped ratio, respectively; the crosses show the measured AMS ratio outside the SAA.

between QT fluxes observed inside and outside the SAA and simply refer to the populations at the altitude of AMS orbit as Quasi-Trapped and Stably Trapped.

[26] The AMS observations differ from the previous measurements at lower energy of the MEPHI group using the Marya instrument [*Galper et al.*, 1986, 1996; V. V. Mikhailov, personal communication, 2001], also shown in Figure 9. These data indicate a strong electron abundance inside the SAA and equivalent fluxes of positrons and electrons outside SAA. In particular, e^- fluxes observed by AMS and Marya outside the SAA agree reasonably well, while the extrapolation to low energy of AMS e^+ fluxes indicates a significantly higher flux with respect to Marya data, which explains the difference observed in the charge ratio (Figure 10a). For the regions inside the SAA, Marya data refer to the Stably Trapped population in the full IVA belts and attention must be paid in the comparison of the two sets of data; AMS observed two different populations and only the ST component is comparable to the MEPHI data, where the QT component is absent. For the ST component, e^+ fluxes agree quite well with lower energy Marya data, while the extrapolation of e^- flux measured by AMS is significantly lower than MEPHI flux, visible in the charge ratio.

[27] Magnetic east/west asymmetries in the QT and ST integral fluxes have been also investigated. In fact, at low altitudes, such asymmetries have been observed in trapped protons [*Heckman and Nakano*, 1963; *Kruglanski and Heynderickx*, 1999] and possibly exist also for leptons.

[28] In a local reference frame with z axis along $\vec{B}$ and the x axis directed as the gradient normal to B, the intrinsic azimuthal β_o angle allows for the separation between particles arriving from the local magnetic east/west. According to this definition, particles from west (east) have always $\beta_o < 0$ ($\beta_o > 0$).

[29] The east/west flux asymmetry A is defined as $A = (J_{\beta_o<0} - J_{\beta_o>0})/(J_{\beta_o<0} + J_{\beta_o>0})$. It is shown as a function of L, for QT and ST lepton components in Figures 11a and 11b, respectively.

[30] The east/west asymmetry is due to the different atmospheric drag experienced by particles from east and from west, acting on very long timescales compared to the drift period [*Walt*, 1964; *Shultz and Lanzerotti*, 1974]. The anisotropy is small and compatible with zero within the errors in the QT component (Figure 11a). This is because their residence time, limited below 30 s, is short with respect to timescale needed to set up the asymmetry; for this reason, transient effects from the production process in atmosphere wash out the asymmetry.

[31] Conversely, the ST fluxes (Figure 11b) are anisotropic at low L values, with an excess of westward ($\beta_0 > 0$, $A < 0$) positrons and of eastward ($\beta_0 < 0$, $A > 0$) electrons, especially at equatorial regions. At high L values, the asymmetry tends to zero as expected from geomagnetic cutoff effects. This is possibly related to the long residence time of the ST component; in this case, more intense long-term effects due to the interactions with the residual atmosphere remove the particles with the guiding centers below the observation point, i.e., e^- from west and e^+ from east. Integral fluxes for the AMS orbit have been investigated also using the invariant radius and latitude, (R_m, Λ_m), representation, which gives the spatial distribution of the particles around the Earth [*Roederer*, 1970].

[32] Each measured pitch angle was converted to the value that would be observed on the same L at a fixed value of $R_m = R_1$. For the AMS circular orbit at $R \sim 400$ km, a value of $R_1 = 1.08R_E$ was adopted, close to the upper limit of R_m where only a small fraction of particles mirrors at higher altitude. The flux intensity at R_1 is related to the local intensity by Liouville's theorem and it is given by $j(E, \alpha_1, L, t) = j(E, \alpha, L, t)$, with the new pitch angle α_1 related to the observed α by $\sin^2 \alpha_1 = K \sin^2 \alpha$, with $K = (B_o L^3/BR_1^3)\sqrt{4 - 4R_1/L}$ [*Selesnick et al.*, 1995]. Knowing the flux map at R_1, it is possible to convert the integral radial flux in a (R_m, Λ_m) map. The limiting assumption is that there are no particles with mirror points above AMS altitude. This can bring to an underestimation of the real flux for possible radial diffusion and loss mechanisms. The results are shown in Figure 12 for QT and ST electrons (Figures 12a and 12b) and positrons (Figure 12c and 12d). It is visible a smooth radial profile for the QT populations with positrons exceeding the electrons (Figures 12a and 12c). The ST fluxes present a different picture, with a slot region in all distributions and a maximum excess of the positrons over electrons at $L \sim 1.3$ (Figures 12b and 12d).

4. Systematic Errors

[33] To evaluate the errors in the particle classification induced by the experimental uncertainties, we performed the following checks. To take into account the errors on initial conditions, we smeared the measured rigidity R and direction by their experimental uncertainties ($\sigma_R \sim 8\%$

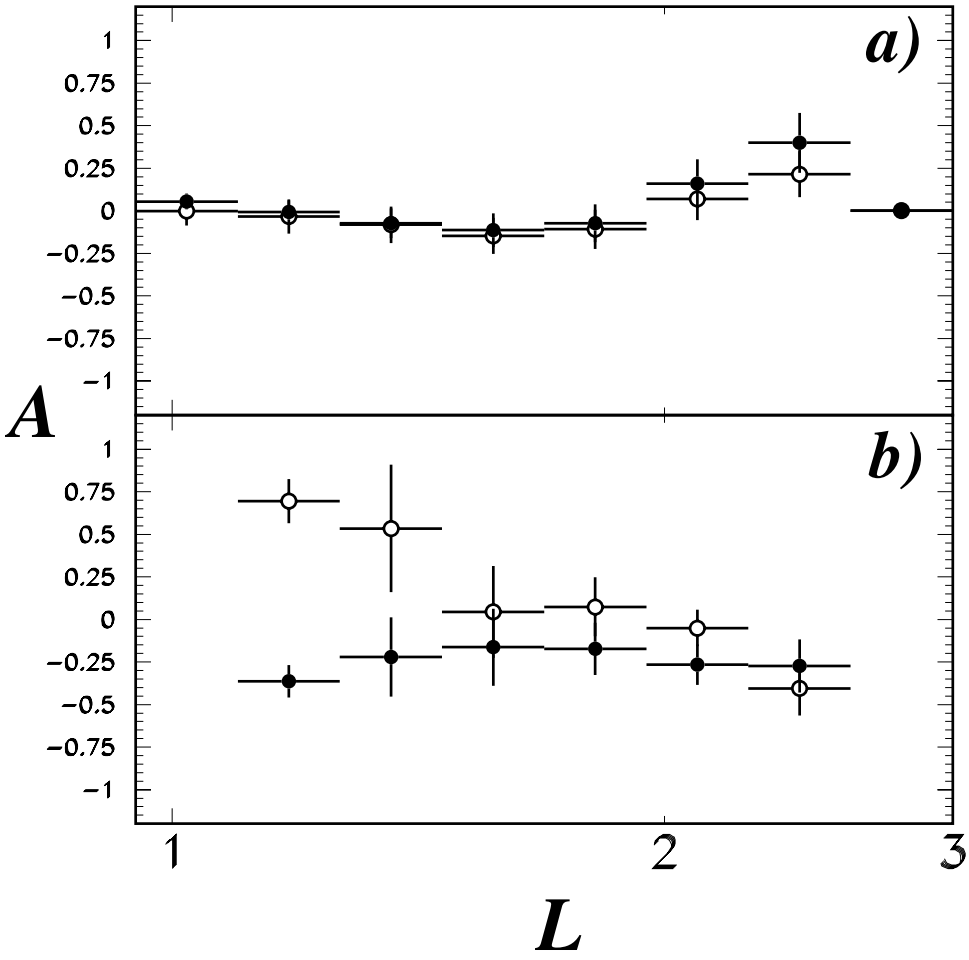

Figure 11. Asymmetry in the integral flux. Quasi-Trapped e^+ (solid circles) and e^- (open circles) irrespective of location are shown in Figure 11a. Stably Trapped positrons (solid circles) and electrons (open circles) inside SAA are shown in Figure 11b.

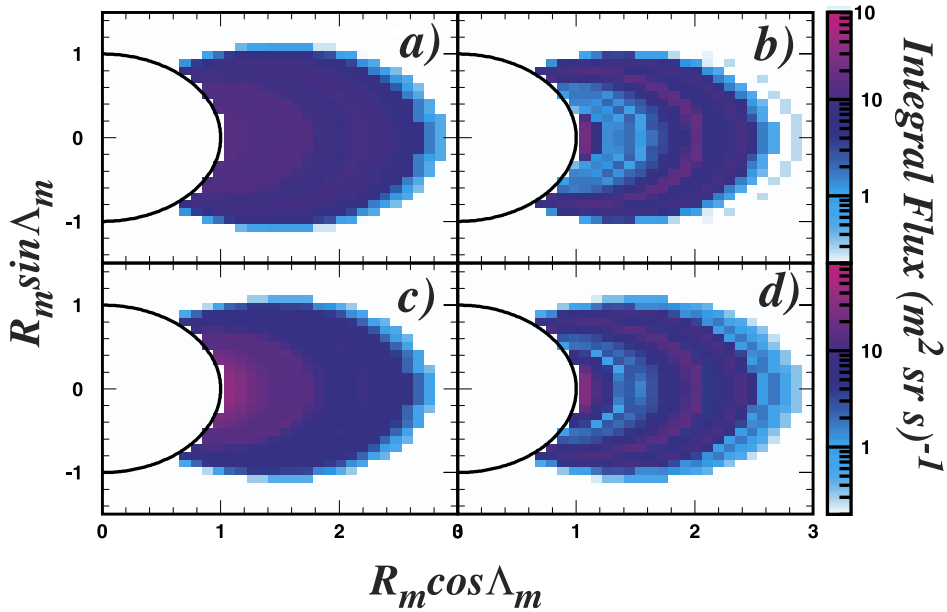

Figure 12. Integral omnidirectional flux maps in (R_m, Λ_m) coordinates for QT and ST (a, b) electrons and (c, d) positrons. The energy intervals are E = 0.205/2.73 GeV. The circles represent the approximate R_m value of the Earth's atmosphere in the SAA region.

Table 2. Systematic Errors Induced by Experimental Uncertainties on the Total Flux J for $0.2 < E < 2.7$ GeV for the Selected Primaries, Quasi-Trapped and Stably Trapped

	$J\ (m^2 srs)^{-1}$	$(\delta J)_{\delta R=1\sigma}$ (%)	$(\delta J)_{\delta\theta=1\sigma}$ (%)	$(\delta J)_{\Delta E=+10\%}$ (%)	$(\delta J)_{Comb}$ (%)
PR($R \geq R_{cu}$)	200.1	−3.58	−0.11	−4.23	−3.74
QT($R \leq R_{cl}$)	134.82	5.23	0.24	6.41	5.31
ST($R \leq R_{cl}$)	23.78	0	−5.47	−4.23	−4.69

below 10 GV, $\sigma_\theta \sim 3.5°$ at $R \sim 200$ MV); an average correction was applied also to each particle for the energy losses in the detector (∼10%). The uncertainties were applied first separately and then simultaneously.

[34] The flux variations for primaries, QT and ST between 0.2 and 2.7 GeV are given in Table 2. It can be seen that the flux variations for the selected particle populations (QT and ST with $R \leq R_{cl}$) are small, so that the overall particle classification is stable against the measurement errors. A relevant feature is that there is not mixing between cosmic and secondary particles (QT and ST) but there a migration from ST to QT populations. The overall penumbra population does not vary appreciably, but migrations are observed among the populations in this region, as expected from the chaotic, nonlinear behavior of the trajectories.

[35] The contribution of the systematic errors to the integral fluxes as a function of L are shown in Figure 5 together with the statistical ones. The sign and the size of the systematic error is given by the pin at the appropriate error bar end of the flux. The systematic error is comparable to the statistical one with a quasi-constant positive sign for QT and negative sign for the ST populations.

[36] The errors play a role around and above the rigidity cutoff R_{cl}, where the adiabatic approach does not hold because of chaotic effects but this region is excluded by the application of the effective cutoff R_{cl}. We conclude that the errors do not introduce relevant bias in the sample of selected particles and the penumbra region is properly removed by the effective cutoff.

5. Conclusion

[37] AMS has measured lepton fluxes in the GeV range in the SAA with good statistical precision. The observations support the existence of a transition region from Stably Trapped to Quasi-Trapped populations at the altitude of AMS orbit. The transition region in the (L, α_o) plane is defined between the lower limit for stable trapping, given by the equatorial drift loss cone angle, α_{st}, and the upper limit, α_{IVA} of the full IVA belts. This region, identified as the mixed radiation belt, may be, at least partly, the source of the injection and loss of high energy particles populating the IVA belts. The transition between ST and QT populations may be attributed to Coulomb scattering in the residual atmosphere, which alters particle pitch angle, allowing them to drift in closed shells. The probability of scattering depends on the average amount of matter crossed by the particle during its motion. The QT fluxes measured inside and outside the SAA are very similar, which indicates that the two fluxes are the same population observed on different points of the drift shell.

[38] The features of the two components, ST and QT, are different. The ST fluxes display a minimum between two different regions: the lower L region dominated by Coulomb losses while at higher L values the radial diffusion possibly dominates. The ST flux, limited to relatively low energy (approximately hundreds of MeV), is detected only in a narrow region corresponding to the inner region of SAA in AMS data. In general, positrons are more abundant than electrons, with a more pronounced dominance in the QT flux.

[39] The origin of the QT flux can be identified with secondaries produced in the atmosphere by the interaction of primary cosmic rays. In this picture the positron dominance is the combined result of the interaction features and of geomagnetic effects [*Huang*, 2003; *Derome et al.*, 2001] (P. Zuccon, A Monte Carlo simulation of the cosmic rays interactions with the near-Earth environment, unpublished, http://ams.pg.infn.it/Tesi/Tesi.html, 2002). The observation of a positron dominance also in ST fluxes suggests that similar sources are the origin of this component, with possibly different injection mechanisms.

[40] The Quasi-Trapped component does not show appreciable anisotropy, because the residence time is much shorter than the time needed to generate asymmetry. This is not true for the Stably Trapped flux, where clear anisotropies are observed at low L shell values. Here long-term interactions with residual atmosphere play an important role in removing particles with guiding centers below the observation point and a steady eastward/westward motion may establish in the belts, in a similar way as for the low-energy ring current.

[41] **Acknowledgments.** We gratefully acknowledge our colleagues in AMS, in particular V. Choutko for his help in the event selection. We greatly benefit of the software libraries (UNILIB, SPENVIS) developed in the context of the Trapped Radiation Environment Development (TREND) project for ESTEC, and we thank D. Heynderickx for his help. This work has been partially supported by Italian Space Agency (ASI) under the contract Asi I/R/211/00.

[42] Lou-Chuang Lee thanks Minghuey Alfred Huang for assistance in evaluating this paper.

References

Akimov, V. V., et al., The main parameters of gamma ray telescope GAMMA-I, in *Proceedings of the 20th International Cosmic Ray Conference*, vol. 2, pp. 320–323, Moscow, Russia, 1987.

Alcaraz, J., et al., The AMS collaboration, leptons in near orbit, *Phys. Lett. B*, *484*, 10–22, 2000.

Averin, S. A., et al., High-energy electrons in the Earth's radiation belt, *Kosmich. Issledov.*, *26*(2), 322, 1988.

Badhwar, G. D., et al., Radiation dose from reentrant electrons, *Radiat. Meas.*, *33*, 369–372, 2001.

Derome, L., et al., Origin of the high energy proton component below the geomagnetic cutoff in near orbit, *Phys. Lett. B*, *489*, 1–8, 2000.

Derome, L., et al., *27th International Cosmic Ray Conference*, p. 174, Copernicus Gesellschaft, Hamburg, Germany, 2001.

Fiandrini, E., G. Esposito, B. Bertucci, B. Alpat, R. Battiston, W. J. Burger, G. Lamanna, and P. Zuccon, Leptons with $E \geq 200$ MeV trapped in Earth's radiation belts, *J. Geophys. Res.*, *107*(A6), 1067, doi:10.1029/2001JA900151, 2002.

Fung, S. F., Recent developments in the NASA trapped radiation models, in *Radiation Belts: Models and Standards*, *Geophys. Monogr. Ser.*, vol. 97, edited by J. F. Lemaire, D. Heynderickx, and D. N. Baker, AGU, Washington, D. C., 1996.

Galper, A. M., et al., Discovery of high energy electrons in the radiation belt by devices with gas cherenkov counters, *Nucl. Instrum. Methods Phys. Res., Sect. A*, *248*, 238, 1986.

Galper, A. M., et al., Electrons with energy exceeding 10 Mev in the Earth's radiation belt, in *Radiation Belts: Models and Standards*, *Geophys. Monogr. Ser.*, vol. 97, edited by J. F. Lemaire, D. Heynderickx, and D. N. Baker, pp. 129–133, AGU, Washington, D. C., 1996.

Gusev, A. A., and G. I. Pugacheva, Formation of albedo electron fluxes in the geomagnetic field, *Geomagn. Aeron.*, *22*(6), 754, 1982.

Heckman, H., and G. Nakano, East-west asymmetry in the flux of mirroring geomagnetically trapped protons, *J. Geophys. Res.*, *68*, 2117, 1963.

Heynderickx, D., M. Kruglanski, J. F. Lemaire, and E. J. Daly, A new tool for calculating drift shell averaged atmospheric density, in *Radiation Belts: Models and Standards*, *Geophys. Monogr. Ser.*, vol. 97, edited by J. F. Lemaire, D. Heynderickx, and D. N. Baker, pp. 173–178, AGU, Washington, D. C., 1996.

Hilton, H., L parameter: A new approximation, *J. Geophys. Res.*, *76*, 6952, 1971.

Huang, M. A., Atmospheric secondary particles in near Earth space, in *Eighth Asia Pacific Physics Conference*, World Sci., River Edge, N. J., in press, 2003.

Il'in, V. D., et al., Stochastic instability of charged particles in a magnetic trap, *Cosmic Res., Engl. Transl.*, *24*, 69–76, 1986.

Kruglanski, M., and D. Heynderickx, Analysis of the low-altitude proton flux asymmetry: Methodology, *Radiat. Meas.*, *30*, 378–382, 1999.

Lemaire, J., et al., TREND3, Radiation environments of astronomy missions and LEO missions, *ESTEC Contract 10725/94/NL/JG(SC)*, Belgian Inst. for Radiat. Anal., Brussels, Belgium, 1998.

McIlwain, C. E., Coordinate for mapping the distribution of magnetically trapped particles, *J. Geophys. Res.*, *66*, 3681, 1961.

Roederer, J. G., *Dynamics of Geomagnetically Trapped Radiation*, Springer-Verlag, New York, 1970.

Selesnick, R. S., A. C. Cummings, J. R. Cummings, R. A. Mewaldt, E. C. Stone, and T. T. von Rosenvinge, Geomagnetically trapped anomalous cosmic rays, *J. Geophys. Res.*, *100*, 9503–9518, 1995.

Shultz, M., and L. J. Lanzerotti, *Particle Diffusion in the Radiation Belts*, Springer-Verlag, New York, 1974.

Tsyganenko, N. A., Determination of magnetospheric model, *Planet. Space Sci.*, *30*, 1982.

Vette, J. I., The AE8 Trapped electron model environment, *NSSDC/WDC-A-R & S 91-24*, Natl. Space Sci. Data Cent., Greenbelt, Md., 1991.

Voronov, S. A., et al., Mariya experience on the analysis of the electron-positron component of cosmic rays onboard the salyut 7, soyuz T-13, kosmos 1669 orbital complex, *Izvest. Vysshikh Uchebnykh Zavedenii Fiz.*, *9*, 19, 1986.

Voronov, S. A., et al., High-energy E: Electrons and positrons in the earth's radiation belt, *Geomagn. Aeron.*, *27*(3), 424, 1987.

Voronov, S. A., et al., Nature of high-energy electrons in Earth's radiation belts, *Cosmic Res.*, *33*, 497–499, 1995.

Walt, M., The effects of atmospheric collisions on geomagnetically trapped electrons, *J. Geophys. Res.*, *69*, 3947–3958, 1964.

B. Alpat, G. Ambrosi, R. Battiston, B. Bertucci, W. J. Burger, D. Caraffini, C. Cecchi, L. Di Masso, N. Dinu, G. Esposito, E. Fiandrini, M. Ionica, R. Ionica, G. Lamanna, M. Menichelli, M. Pauluzzi, and P. Zuccon, Department of Physics, Perugia University, Via Pascoli, I-06100 Perugia, Italy. (emanuele.fiandrini@pg.infn.it)